Mechanical properties and thermal stability of hot-rolled Al–15%B_4C composite sheets containing Sc and Zr at elevated temperature

Jian Qin, Zhan Zhang, X.-Grant Chen *

Department of Applied Science, University of Quebec at Chicoutimi,

Chicoutimi, (QC), Canada G7H 2B1

Abstract

The microstructure, mechanical properties, thermal stabilityand tensile fracture of two hot-rolled Al-15 vol.% B_4C composite sheets (S40 with 0.4 wt.% Sc and SZ40 with 0.4 wt.% Sc and 0.24 wt.% Zr) were investigated. During multi-pass hot rolling, coarse Al_3Sc or Al_3(Sc, Zr) precipitations appeared and resulted in the loss of most of their hardening effect. In an appropriate post-rolling heat treatment, the hot-rolled sheets regained a significant precipitation hardening because of the precipitation of fine nanoscale Al_3Sc and Al_3(Sc,Zr) that uniformly distributed in the aluminum matrix. After the peak aging, the ultimate tensile strength at ambient temperature of the S40 and SZ40 sheets can reach 198 MPa and 215 MPa, respectively. During 2000 h of annealing at 300 ºC, the strengths at ambient temperature of both S40 and SZ40 composite sheets slowly decreased with increasing annealing time. However, the tensile strengths at 300 ºC of both S40 and SZ40 composite sheets remained nearly unchanged and were less sensitive to the annealing time and more tolerable for precipitate coarsening, which demonstrated an excellent long-term thermal stability of both materials at elevated temperature. The tensile fracture at ambient temperature of both S40 and SZ40 composite sheets was

dominated by the brittle B_4C particle fracture, whereas the interfacial decohesion of B_4C particles became the prominent characteristic of the fracture at 300 ºC.

Keywords: Al-B_4C composites; Mechanical properties; Thermal stability; Post-rolling teat treatment; Fracture

* Corresponding author:

X.-Grant Chen, Tel.: 1-418-545 5011 ext. 2603; Fax: 1-418-545 5012;

E-mail: xgrant_chen@uqac.ca

1. Introduction

Aluminum-based metal matrix composites (MMCs) have been widely used in automotive, aerospace and military industries as either structural or functional materials because of their light weight, high specific modulus, low coefficient of thermal expansion and other special properties [1]. As a neutron absorption material, Al–B_4C composites are applied to fabricate the transport and storage containers of spent nuclear fuels because of the special capacity for capturing neutrons [2, 3]. In service, Al–B_4C composites absorb the neutrons and generate heat and hence it can expose to elevated temperatures (250-350 °C) for an extended period [4, 5]. It demands that the material can maintain its mechanical properties and thermally stability at such temperatures. Sc was introduced to aluminum alloys to enhance the mechanical properties by forming fine coherent Al_3Sc precipitates with a low coarsening rate (stable up to 300 °C) [6]. The addition of Zr can further reduce the coarsening rate of the precipitates [7, 8], improve the thermal stability of precipitates (stable up to 350 °C) [7] and increase the strength and recrystallization resistance [9-11]. Therefore, the Al–Sc and Al–Sc–Zr matrix are promising candidates to develop advanced Al–B_4C composites that are applicable at elevated temperatures.

In recent years, several researchers put great efforts into understanding the strengthening behavior and creep properties of Al–Sc and Al–Sc–Zr cast alloys [11-13]. The mechanical properties at room and elevated temperatures of Al–B_4C cast composites that contain Sc and Zr were investigated in our previous works [14-16]. Al_3Sc and $Al_3(ScZr)$ precipitates could strengthen Al–B_4C cast composites and were thermally stable up to 300ºC. To manufacture useful engineering final products, Al–B_4C cast composites need to undergo the hot-working processes such as rolling, extrusion and forging. It was reported that Al_3Sc precipitation hardening in deformed materials was difficult because of severe limits on the solution treatment,

hot deformation and post heat treatment [17]. In our previous work [18], we found that the strengthening solute atoms (Sc) in an Al–B_4C composite would be consumed during the post-rolling solution heat treatment, and the consumption of Sc increased with the increase in deformation ratio. In general, the public information about the hot deformation process, post-deformation heat treatment, and microstructure evolution for Al–Sc and Al–Sc–Zr alloys is notably scarce. Furthermore, notably few papers address the mechanical properties at elevated temperature of final deformed Al–Sc alloys and deformed Al–B_4C composites that contain Sc and Zr.

The damage and failure modes of composite materials are important aspects for an engineering product. The failure mechanism of particulate-reinforced MMCs can be classified into three types: reinforcement fracture when the matrix is stronger than the reinforcement [19, 20]; interfacial decohesion when the bonding force is lower than the matrix and reinforcement [21, 22]; ductile failure because of the void coalescence of the matrix [23, 24]. However, the fracture behavior at elevated temperature for Al–B_4C composites is little known.

In the present work, the mechanical properties as a function of temperature and the evolution of mechanical properties during long-term annealing at 300 °C for two hot-rolled Al–15 vol.% B_4C composite sheets containing Sc and Zr were investigated. The effect of the post-rolling heat treatment on the Al_3Sc and $Al_3(Sc,Zr)$ precipitation hardening was studied. The evolution of Al_3Sc and $Al_3(ScZr)$ precipitates in rolled sheets during long-term annealing was observed. In addition, the effect of the testing temperatures on the fracture behavior of two hot-rolled Al–B_4C composite sheets was studied.

2. Experimental Procedure

In the present work, two experimental Al 1100–15 vol. % B_4C composites were prepared in an electric resistance furnace to obtain the desirable chemical composition: S40 with 0.4 wt.% Sc and SZ40 with 0.4 wt.% Sc plus 0.24 wt.% Zr. The average size of the B_4C particles was 23 μm. Their nominal chemical compositions are listed in Table 1. Under mechanical stirring using an impeller, the composite melt was held at 740 °C for 30 min. and subsequently poured into a rectangular permanent steel mold that measured 30×40×80 mm. The cast ingots of two composites were homogenized at 640 °C for 24 hours (S40) and 96 hours (SZ40), respectively, and quenched in water at room temperature. Then, the cast ingots were hot-rolled on a laboratory scale rolling mill (STANAT CX-100) with multi-passes in a temperature range of 400 to 500 °C. The rolling began from the 30 mm thick original ingot and ended at the 4 mm sheets with a total reduction ratio of 87%. After hot rolling, the composite sheets were solution-treated at 640 °C for different time lengths, quenched with water at room temperature, and aged at 300 °C for 24 hours. To assess the long-term thermal stability of the mechanical properties, the heat-treated sheets were annealed at 300 °C for up to 2000 hours.

Table 1 Nominal chemical composition of the experimental composites

Code	Element (wt.%)				
	Sc	Zr	Ti	B_4C (vol.%)	Al
S40	0.40	–	1.50	15	Balance
SZ40	0.40	0.24	1.50	15	

The tensile properties were measured with an Instron machine according to the ASTM E8M-04 standard for room temperature and ASTM E21 standard for elevated temperature. The ultimate tensile strength (UTS), 0.2% yield strength (YS) and elongation at fracture (EL) were averaged over three tests for each condition. The tensile samples with an overall length of 100

mm and the gage gauge length of 25 mm and width of 6 mm were machined from the rolled sheets based on ASTM E8M-04 standard.

The microstructure of the composites was observed using an optical and scanning electronic microscope (SEM, JSM-6480LV), which was equipped with an electron backscatter diffraction system (EBSD) and an energy dispersive spectrometer (EDS). The fracture surfaces of the tensile samples were examined using SEM. A transmission electron microscope (TEM, JEM-2100) that operated at 200 kV was used to observe the precipitates Al_3Sc and Al_3(Sc Zr). Centered dark-field images of the precipitates were recorded using the {100} super-lattice reflections near the <011> direction. Two-beam diffraction conditions were applied for the precipitate observation. The precipitate equivalent diameters were determined using image analysis on the TEM images.

3. Results and Discussion

3.1 Microstructure of the as-cast and as-rolled composites

The as-cast microstructure of the composites in an example S40 is shown in Fig. 1. B_4C particles were generally uniformly distributed in the aluminum matrix, and some small interfacial reaction particles [25] were also visible, attached or surrounded on the B_4C particles (Fig. 1a). After etching, the aluminum matrix of composites evidently consisted of coarse and equiaxed grains with an average size of 100 to 130 μm.

During the multi-pass hot rolling, the composite materials experienced repeated work hardening, dynamic recovery and dynamic recrystallization. The EBSD mapping images (Fig. 2) show the as-rolled grain structures at the 87% deformation ratio (4 mm sheets). The grains were arranged along the rolling direction, and the grain sizes were much smaller than the as-cast

grains. In addition, a large amount of sub-grains and dislocation bands with a misorientation less than 15° were created in both S40 and SZ40 samples.

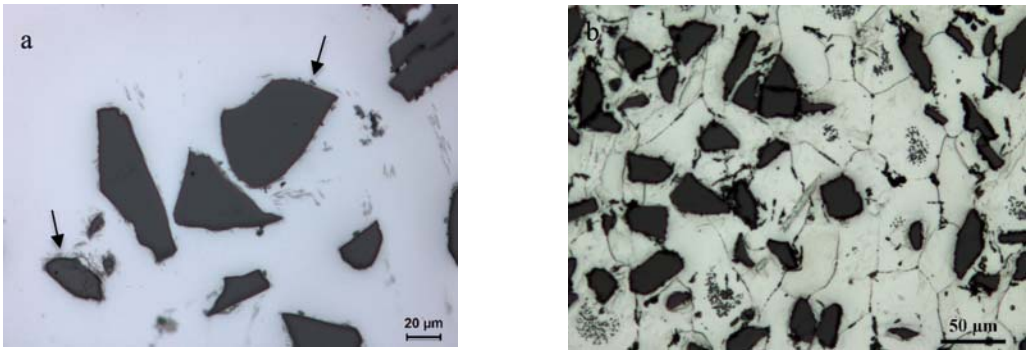

Fig. 1. Optical microstructure of the as-cast S40 composite (a) with arrows pointing to the small interfacial reaction particles that surrounded the B_4C particles, and the etched sample shows equiaxed grains of the Al matrix (b).

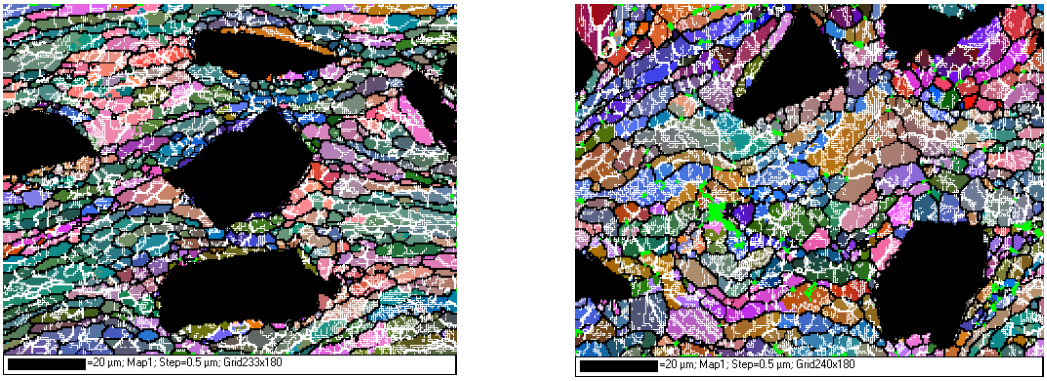

Fig. 2. EBSD mapping shows the grains and subgrain structures in the 4 mm as-rolled S40 sheet (a) and SZ40 sheet (b). The black regions are B_4C particles. The other colors indicate the grains or subgrains with misorientations: thin white lines: 1~5°; white lines: 5~15°; black lines: >15°.

3.2 Post-rolling heat treatment

After hot rolling, the as-rolled sheets were notably soft. To gain the appropriate mechanical properties as useful engineering materials, the as-rolled materials experienced a post-rolling heat treatment, which involved both solution and aging for precipitation hardening. To find the optimal heat treatment, the solution treatment was performed at 640 ºC with different holding time lengths and a subsequent fixed aging treatment at 300 ºC for 24 hours, which was identified as the peak aging condition for Al-Sc-B_4C and Al-Sc-Zr-B_4C composites [14]. The Vickers' hardness of the aluminum matrix of both composite sheets as a function of the solution time is shown in Fig. 3. The hardness values of the S40 and SZ40 composites in the as-rolled condition were 39 and 42 HV, respectively, which showed a low strength of the materials after hot rolling. After only one hour of solution treatment, the hardness increased to 62 HV for S40 and 70 HV for SZ40. These peak values were maintained for approximately three and six hours for S40 and SZ40, respectively. After the peak aging plateau, the hardness gradually decreased with increasing solution time.

During the multi-pass hot rolling, the homogenized composite ingots experienced a repeated thermomechanical annealing process at 400-500 °C. The solutes of Sc and Zr precipitated from the supersaturated aluminum matrix in the forms of Al_3Sc or Al_3(Sc Zr) precipitates. However, because of the high precipitation temperature, those precipitates were notably coarse: their diameters were tens to hundred nanometers (Fig. 4a). In addition, many of them were on the grain or sub-grain boundaries, which resulted in the loss of most of their hardening effect. The results in Fig. 3 suggest that the solution treatment of rolled composite sheets in a relatively short time (~ one hour) can dissolve these coarse precipitates back to the aluminum matrix, which ensures the re-precipitation of much fine precipitates during subsequent aging and regains the

strength of the rolled composite sheets. Fig. 5 shows the precipitates in S40 and SZ40 that were solution-treated at 640 ºC for three hours and aged at 300 ºC for 24 hours. The fine nanoscale precipitates uniformly distributed in the aluminum matrix. The average diameters of the precipitates were 2.8 nm (Al_3Sc in S40, Fig. 5a) and 3 nm ($Al_3(Sc,Zr)$ in SZ40, Fig. 5b), which resulted in a much higher strength after the post-rolling treatment than that in the as-rolled condition (Fig. 3).

After the post-rolling heat treatment, the sub-grain structure that formed during rolling (Fig. 2) was completely eliminated, and all grains were fully recrystallized (Fig. not showing here). Because of the high solution temperature, the grain structure became notably coarse, and the average grain sizes of S40 and SZ40 were 94 and 42 μm, respectively.

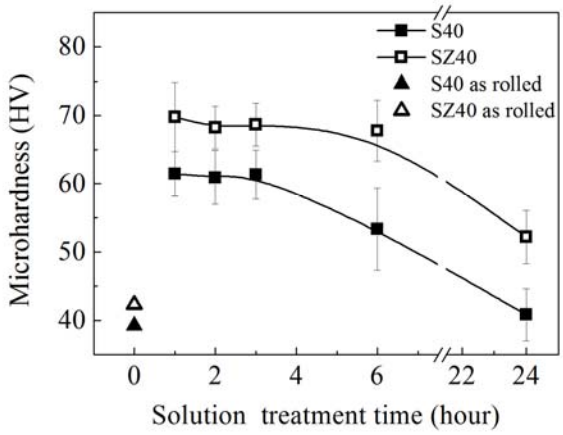

Fig. 3. Vickers' hardness of both composite sheets as a function of the solution time (solution at 640 ºC and aging at 300 ºC/24 h).

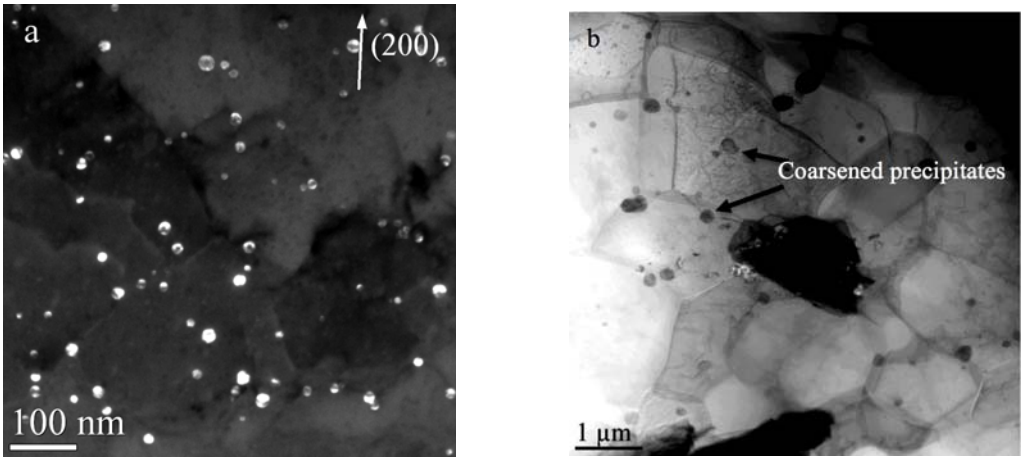

Fig. 4. Dark-field TEM images of the coarse precipitates in SZ40 (a) and STEM image of many coarse precipitates on the grain and subgrain boundaries (b).

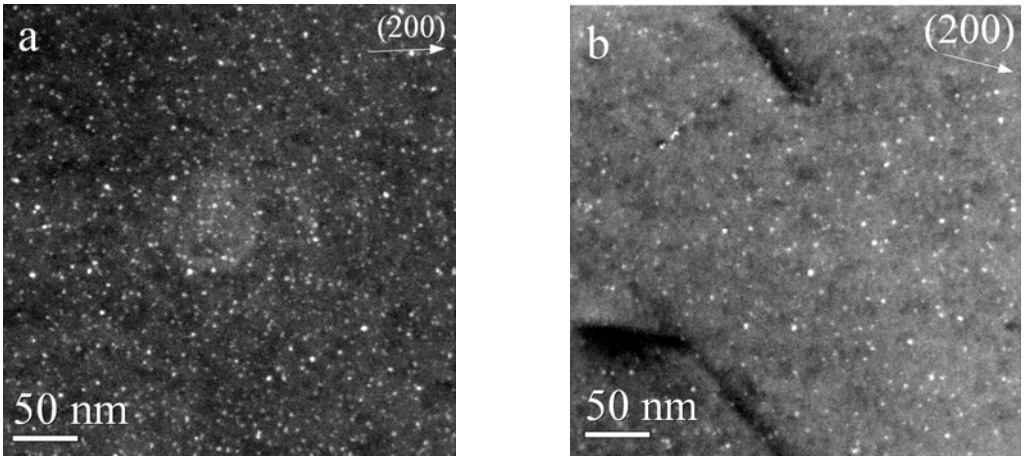

Fig. 5. Fine precipitates in the aluminum matrix of S40 (a) and SZ40 (b) after the peak aging of the rolled sheets (solution-treated at 640 °C/3 h and aged at 300 ºC/24 h)

3.3 Mechanical properties and thermal stability

3.3.1 Tensile properties at different temperatures

The tensile properties of the rolled S40 and SZ40 composite sheets after peak aging were tested at 25 °C, 250 °C and 300 °C. Fig. 6 shows the ultimate tensile strength (UTS), 0.2% offset yield strength (YS) and elongation (EL) of both composite sheets at different test temperatures.

In general, the UTS and YS of both materials decrease, and the EL increases with increasing test temperatures. For example, the UTS and YS of S40 were 197 MPa and 152 MPa at ambient temperature but became 65 MPa and 55 MPa at 300 ºC, respectively. The EL of S40 was approximately 9% at ambient temperature and increased to 30% at 300 ºC. The strength of S40 at 300 ºC was approximately 35% of the strength at ambient temperature whereas the elongation at 300 ºC was approximately 3.3 times of that at ambient temperature. For the SZ40 composite, the UTS and YS at ambient temperature were 210 MPa and 166 MPa, respectively, which were slightly higher than that of S40 at ambient temperature. However, at elevated temperatures (250−300 ºC), the tensile strengths of both composites became close, and the values remained almost constant.

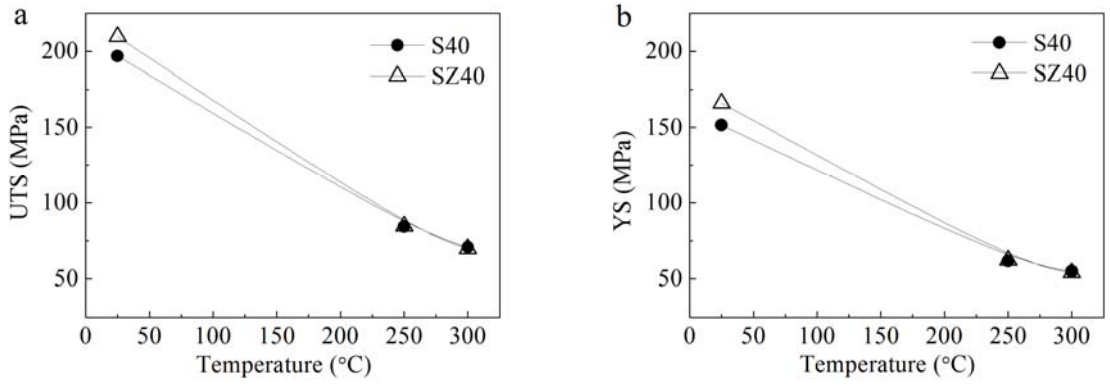

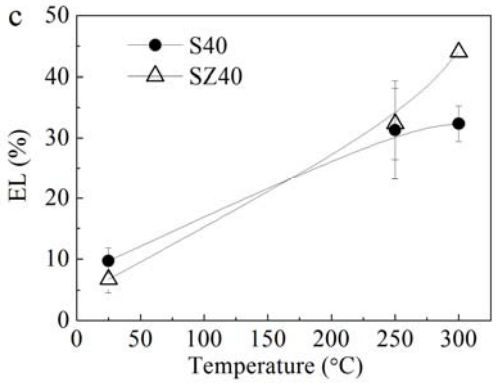

Fig. 6. Tensile properties of the S40 and SZ40 sheets after peak aging as a function of temperature: UTS (a), YS (b) and El (c).

3.3.2 Evolution of tensile properties during long-term annealing

After the peak aging, the S40 and SZ40 composites were annealed at 300 °C for up to 2000 hours to assess the long-term thermal stability of the materials. Fig. 7 shows the mechanical properties of the S40 and SZ40 samples as a function of the annealing time, which were tested at both ambient temperature and 300 °C. The strengths (UTS and YS) at the ambient temperature slowly decreased with increasing annealing time. The UTS of S40 slightly decreased from 197 MPa to 190 MPa, whereas the YS slightly decreased from 152 MPa to 148 MPa after 2000 h of annealing (Figs. 7a and 7c). SZ40 generally has higher strengths than S40 (~15 MPa above) but the strengths exhibit the identical decreasing tendency as S40 during 2000 h of annealing. The EL of both composites did not significantly change during the entire annealing process (Fig. 7e).

At 300 ºC, the UTS and YS and their evolution during annealing for both composites are almost identical (Figs. 7b and 7d). The UTS only slightly decreased from 70 to 65 MPa in the

first 500 h of annealing and subsequently stabilized in the remaining annealing period. The YS was approximately 55 MPa and remained unchanged during the entire annealing process. The elongation of both composites moderately decreased in the first 500 h of annealing and stabilized at approximately ~26% (Fig. 7f). The independence of the UTS and YS from the annealing time at 300 ºC for up to 2000 h indicates the excellent long-term thermal stability of both S40 and SZ40 composite sheets at elevated temperature.

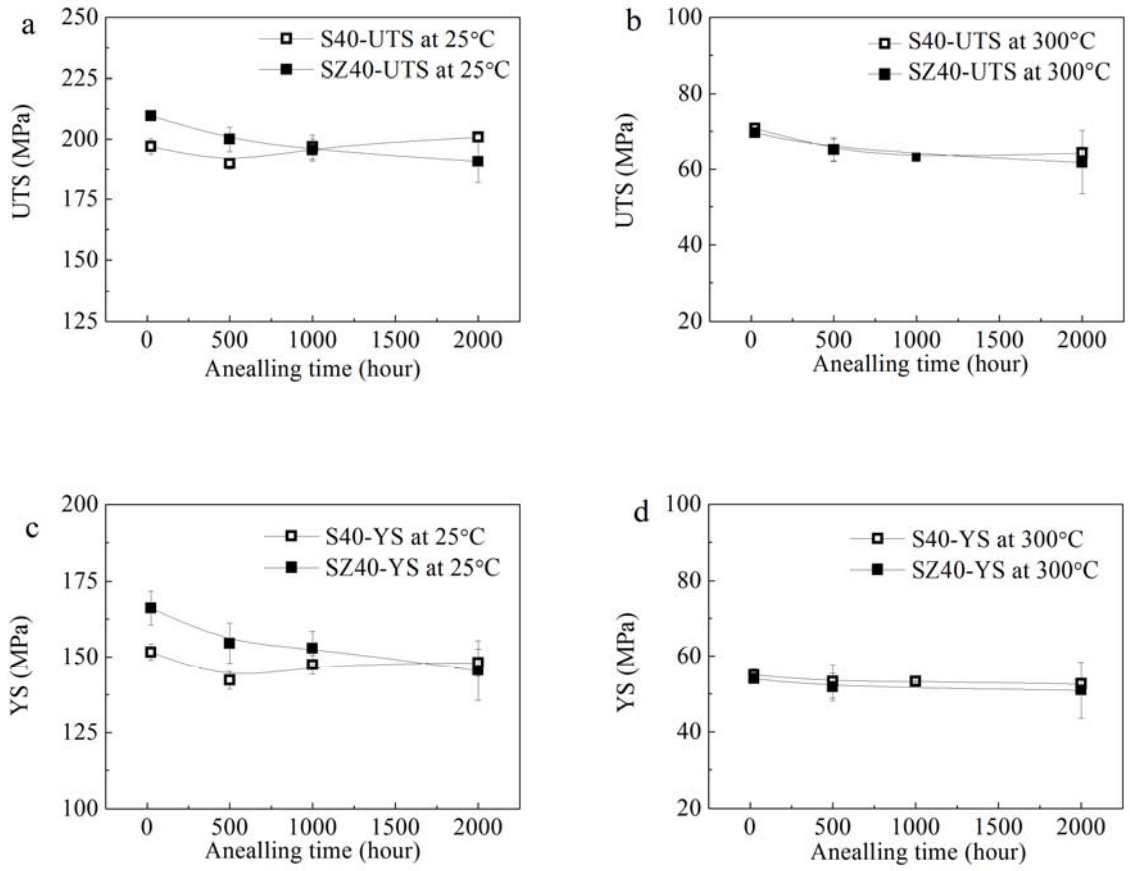

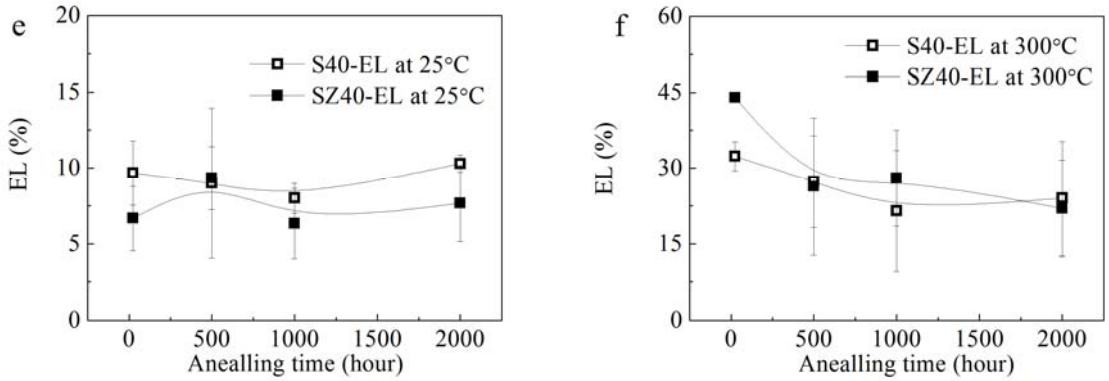

Fig. 7. Evolution of the mechanical properties of both S40 and SZ40 composite sheets during long-term annealing at 300 °C: (a) UTS, (c) YS and (e) EL at 25 °C; (b) UTS, (d) YS and (f) EL at 300 °C.

It is well-known that the AA1100 matrix is a non-heat-treatable material, the strength of which is mainly gained by strain hardening during deformation. After annealing, the AA1100−O matrix is notably soft, and the YS is only 38 MPa at ambient temperature [26], which cannot provide much support to strengthen the Al−B_4C composites. After the alloying with Sc and Zr and the peak aging, the strengths of S40 and SZ40 largely increase because of the precipitation strengthening of nanoscale Al_3Sc and Al_3(Sc Zr) precipitates. The YS at ambient temperature can reach 150 MPa and 165 MPa for S40 and SZ40, respectively. Fig. 8 shows the TEM images of the precipitates after 2000 h of annealing at 300 °C. During long-term annealing, a slow coarsening process occurred for both Al_3Sc and Al_3(Sc Zr) precipitates. Compared to Fig. 5, the average size of Al_3Sc in S40 increased from 2.8 nm to 14 nm (in the diameter), whereas the size of Al_3(Sc Zr) in SZ40 increased from 3 nm to 4.6 nm (in diameter) after 2000 h of annealing. The slow decrease in strengths (UTS and YS) at ambient temperature during long-term annealing is mainly because of the precipitate coarsening. In general, the classical precipitate shearing and

Orowan dislocation bypassing mechanisms can explain the ambient temperature strength in precipitate-strengthening materials [12, 13, 16]. In the case of coarsening during annealing, the precipitates become too large for shearing, and Orowan dislocation bypassing begins to be active. Therefore, the strength decreases with increasing precipitate size under the Orowan dislocation bypassing mechanism.

In certain applications, the mechanical properties and thermal stability of Al–B_4C composites at elevated temperature are highly important [14, 16], which is the main reason for alloying with Sc and Zr. It was reported that, in the absence of precipitate strengthening, the YS at 300 °C was only approximately 14 MPa for the AA1100 matrix [26] and 23 MPa for an AA1100−25% B_4C composite [27], which could not serve as a useful structural material at elevated temperature. In the present study, the YS at 300 °C of both S40 and SZ40 rolled sheets approaches 55 MPa. This improvement is significant for elevated-temperature applications. More importantly, the strength at 300 °C of both S40 and SZ40 sheets are notably stable for at least 2000 h. It brings a highly interesting property for structural applications, which may experience an extended period of exposure to high service temperatures (250−350 °C). In contrast to the strengths at ambient temperature, the strengths (both UTS and YS) at 300 °C are less sensitive to the annealing time and more tolerable for precipitate coarsening. In our recent study [15], a dislocation climb mechanism was proposed to explain the precipitate strengthening at elevated temperatures (> 0.5 T_m), where the elevated temperature strength was much less sensitive to coarse precipitates in a certain range of precipitate sizes. Detailed discussions of precipitate strengthening mechanisms of this composites at elevated temperature can be found in [15]. The experiment results in the present study are consistent with the predication of the dislocation climb mechanism.

It is worthwhile to mention that the Al_3Sc precipitates in S40 have a higher coarsening rate than the $Al_3(Sc,Zr)$ precipitates in SZ40 (Fig. 5 vs. Fig. 8). Results demonstrated that, within 2000 h of annealing, the coarsening of Al_3Sc precipitates in S40 did not affect the tensile strength at 300 °C yet. However, with further prolonged annealing, the coarsening of Al_3Sc certainly continues, and up to some point, the strength of S40 is expected to decrease because of the weaker strengthening effect of coarsened precipitates. However, it is anticipated that the strength of SZ40 at 300 °C is more stable for the annealing much beyond 2000 h because of the low coarsening rate of $Al_3(Sc,Zr)$ precipitates. Thus, the SZ40 composite is more suitable for applications with exposure to high service temperatures for extended periods of time.

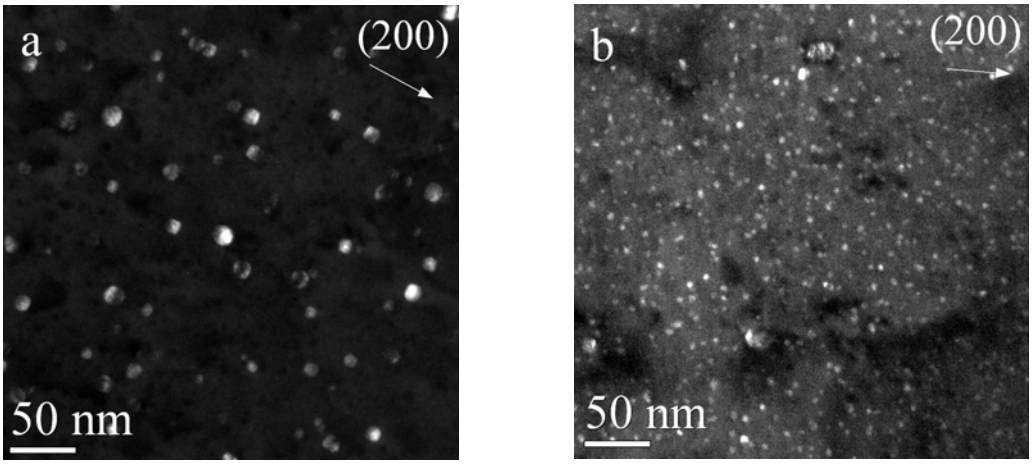

Fig. 8. TEM dark-field images of the coarsened precipitates after 2000 h of annealing in S40 (a) and SZ40 (b).

3.3 Fractography

The fracture surfaces of the tensile samples, which were tested at 25, 250 and 300 ºC, were examined by SEM to study the fracture mechanisms during the tensile deformation. Fig. 9 shows

the typical SEM micrographs of the fracture surfaces of the tested S40 sample at 25 °C. Many ductile dimples in the aluminum matrix and brittle fracture in B_4C particles evidently appeared on the fracture surface (Fig. 9a). The deep dimples in the matrix indicate that plastic deformation occurred before the final failure [28, 29]. The B_4C particle fractures had a cleavage and facet plane (Fig. 9b). In a cross section of the fracture surface, a large crack throughout the B_4C particle was clearly observed (Fig. 9c). When the test temperature increased to 250 °C, two types of dimples were observed in the fracture (Fig. 10): the small and ductile dimples in the matrix, which were several micrometers in size, and the larger dimples that were tens of micrometers in size, which was similar to the B_4C particle size. Small particles appeared at the bottom of the large dimples (Fig. 10b). Ti and Sc were detected in the small particles (Fig. 10c), which indicated that the large dimples were the interface layers between B_4C particles and the aluminum matrix, where the B_4C particles were debonded during the tensile deformation. The interfacial decohesion of B_4C particles was observed in most parts of the fracture surface. However, few B_4C particle fractures were found in the fracture surface (arrow in Fig. 10a), but the amount of broken B_4C particles was less than 10% of B_4C particles. When tested at a higher temperature (300 °C), the fracture surface was only dominated by the interfacial decohesion of B_4C particles and ductile dimples in the matrix (Fig. 11). In the cross section of the fracture surface, the interfacial decohesion of B_4C particle was more evident (Fig. 11c); no more fracture of B_4C particles was found.

The fracture observation of the tested SZ40 samples at different temperatures indicates a similar tendency to that of the S40 samples: the brittle particle fracture and ductile matrix fracture at ambient temperature and the interfacial decohesion and ductile matrix rupture at 300 ºC. Moreover, for both S40 and SZ40 samples after long-term annealing (300ºC/2000h), the

observation of the fracture surface showed that the long-term annealing did not change the fracture behavior because the B_4C ceramic particles and their interfaces with solid aluminum were notably stable at such temperature.

The fracture types of particulate-reinforced MMCs under tensile stress can be classified into three cases [30]: (1) particle fracture, which occurs when the matrix is strong and the local stress exceeds the fracture strength of the reinforcement particle; (2) interfacial decohesion, which is related to the characteristic that the local stress is lower than the particle fracture but higher than the interfacial strength; (3) matrix fracture because of the void coalescence, when both interface and reinforcement are stronger than the matrix. During the tensile deformation of the Al–B_4C composites, the aluminum matrix begins to plastically deform, which is associated with dislocation pile-up near the particle/matrix interfaces. The increase in shear stress at the head of the pile-up can be transferred to the B_4C particles through the interface. With the precipitation of nanoscale Al_3Sc and $Al_3(Sc,Zr)$ precipitates, the UTS of the S40 and SZ40 samples at ambient temperature is notably strong and approximately 200 MPa. During the tensile deformation, the applied local stress appears to exceed the fracture strength of B_4C particles. Cracks can nucleate on the particle surface under the action of the shear stress and easily propagate through the entire particles. After the failure of the B_4C particles, the increase in stress on the matrix causes void growth and coalescence, and the composite sample is finally ruptured with the ductile dimple morphology in the matrix fracture surface. Therefore, the fracture at ambient temperature is dominated by the brittle B_4C particle fracture.

When tested at high temperature (250 °C), the tensile strength of the S40 and SZ40 composites significantly decreased (Fig. 5.6), and the applied stress was not sufficient to fracture most particles but exceeded the interface strength. The interfacial decohesion with partial particle

fracture became the dominant feature for the material failure at 250 ºC. With further increase in test temperature (300 °C), the UTS of the composites decreased again (to approximately 65 MPa). The applied local stress was much lower than the particle strength but remained higher than the interface strength. The main characteristic of the fracture became purely interfacial decohesion. The rupture of the composite at 300 ºC is mainly controlled by the interfacial separation between B_4C particles and the matrix.

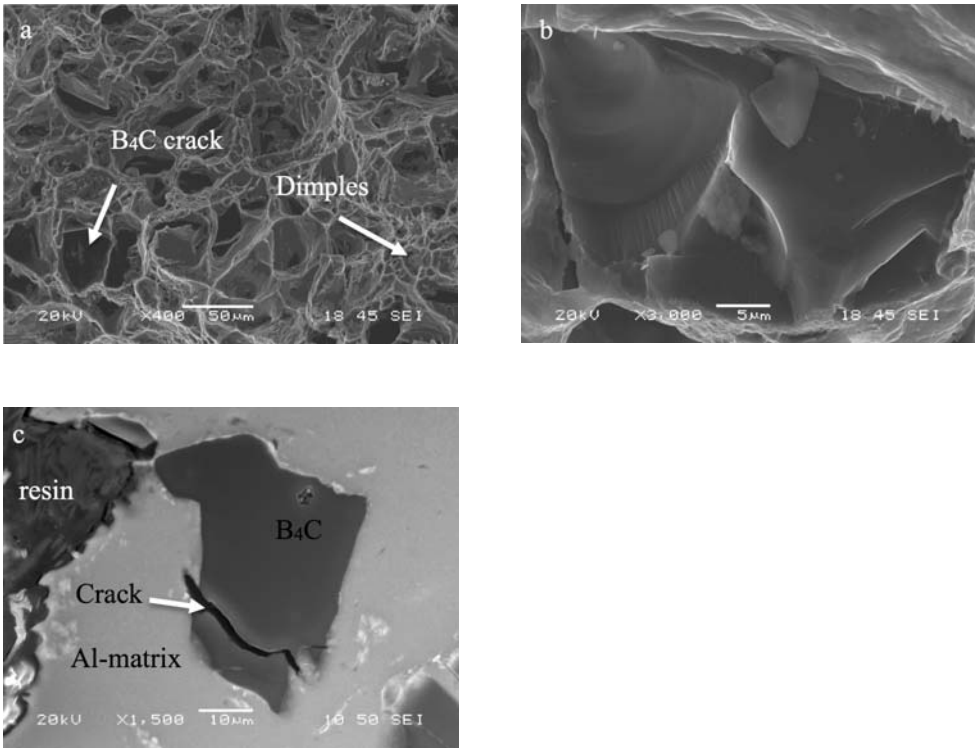

Fig. 9. SEM images of the tensile fracture surface of the tested S40 sample at 25°C: (a) general view; (b) enlarged fracture surface of a B_4C particle; (c) cross-section of the fracture.

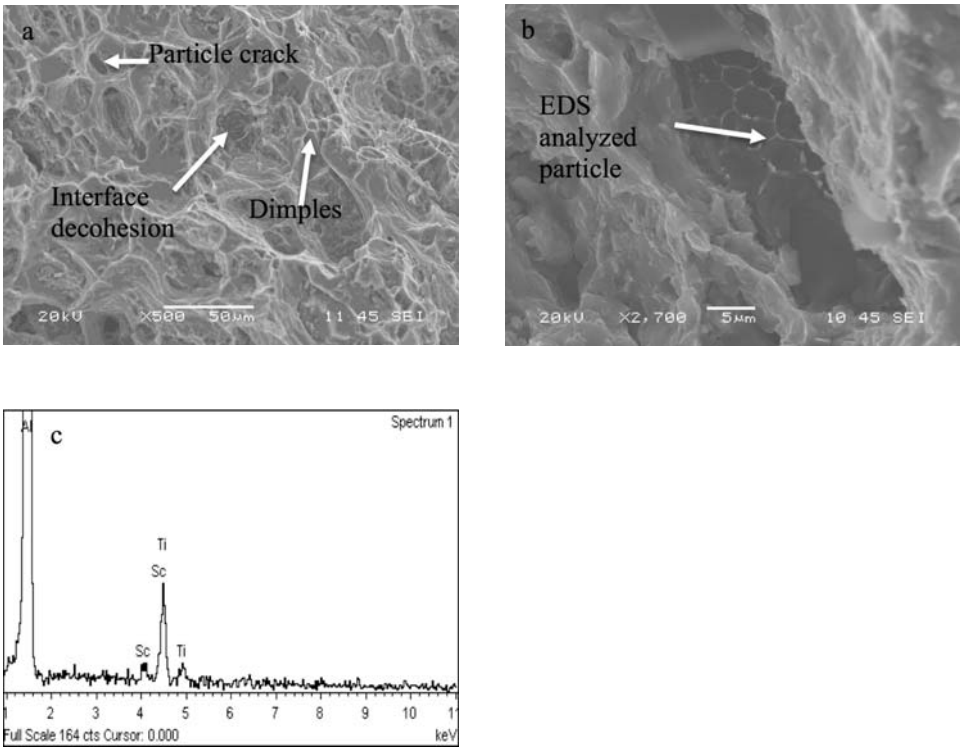

Fig. 10. SEM images of the tensile fracture surfaces of the tested S40 at 250 °C: (a) general view; (b) enlarged view of the interfacial decohesion, where the B_4C particle was out of the matrix; (c) EDS spectrum of a small particle in the interfacial layer.

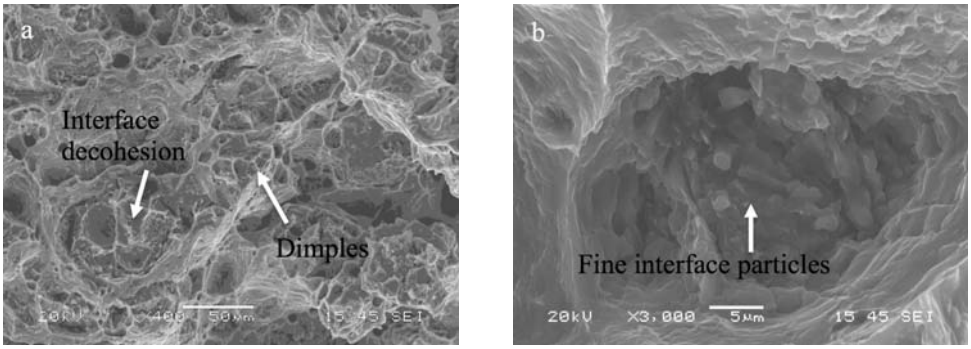

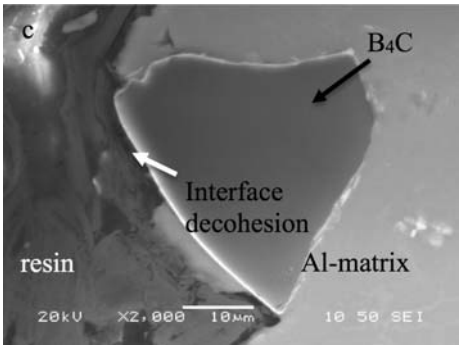

Fig. 11. SEM images of the tensile fracture surfaces of tested S40 at 300 °C: (a) general view; (b) enlarged view of the interfacial decohesion, where the B_4C particle was out of the matrix; (c) cross-section of the fracture.

4. Conclusions

1) With the alloying of Sc and Zr, the hot-rolled Al–15 vol.%B_4C composite sheets can regain a significant precipitation hardening in an appropriate post-rolling heat treatment because of the precipitation of nanoscale Al_3Sc and $Al_3(Sc,Zr)$, which uniformly distribute in the aluminum matrix. After the peak aging, the UTS at ambient temperature of the S40 (Al–15 vol.%B_4C-0.4 wt.%Sc) and SZ40 (Al–15 vol.%B_4C-0.4 wt.%Sc-0.24 wt.%Zr) sheets can reach 197 MPa and 210 MPa, respectively. The tensile strength of both materials decreases with increasing test temperature. The UTSs at 300 ºC of S40 and SZ40 become close and remain at approximately 65 MPa.
2) During 2000 h of annealing at 300 ºC, a slow coarsening process occurs for Al_3Sc (S40) and $Al_3(Sc,Zr)$ (SZ40) precipitates. The strengths at ambient temperature of both S40 and SZ40 composite sheets slightly decrease with increasing annealing time. The UTS at

ambient temperature of S40 changes from 197 to 190 MPa, whereas the UTS of SZ40 decreases from 210 to 191 MPa after 2000 h of annealing.

3) The UTS and YS at 300 ºC of both S40 and SZ40 composite sheets remain almost unchanged during 2000 h of annealing, and they are less sensitive to the annealing time and more tolerable for precipitate coarsening, which shows an excellent long-term thermal stability of both materials at elevated temperature.
4) The tensile fracture mechanism of both S40 and SZ40 composite sheets is temperature-dependent. The fracture at ambient temperature is dominated by the brittle B_4C particle fracture, whereas the interfacial decohesion of B_4C particles becomes the prominent characteristic of the fracture at 300 ºC.

Acknowledgments

The authors would like to acknowledge the financial support of the Natural Sciences and Engineering Research Council of Canada (NSERC) and Rio Tinto Aluminum through the NSERC Industry Research Chair in the Metallurgy of Aluminum Transformation at University of Quebec at Chicoutimi.

References

1. Ibrahim IA, Mohamed FA, Lavernia EJ. Particulate reinforced metal matrix composites - a review. J Mater Sci 1991; 26: 1137-56.
2. Chen XG. Application of Al-B_4C Metal Matrix Composites in the Nuclear Industry for Neutron Absorber Materials. In: Nikhil G, Warren H, editor. Proceedings of solidification

processing of metal matrix composites. San Antonio, USA, TMS Conference 2006. p. 343-50.

3. Bonnet G, Rohr V, Chen XG, Bernier J-L, Chiocca R, Issard H. Use of Alcan's Al-B_4C Metal Matrix Composites As Neutron Absorber Material in TN International's Transportation and Storage Casks. Packag Transp Stor Secur Radioact Mater 2009; 20: 98-102.

4. Yamazaki T, Sanada K, Nishiyama T, Ishii H. Development of Neutron Absorber (Maxus^{Tm}) for High Burn-Up Spent Nuclear Fuel. In: Proceedings of 15th International Symposium on the Packaging and Transportation of Radioactive Materials (PATRAM 2007). Miami, Florida, USA, Conference 2007. p.1149-54.

5. Maeguchi T, Kamiwaki Y, Ishiko D, Yamamoto T. Development and reliability verification of aluminum alloys for basket of transport and storage cask for spent nuclear fuel. In: Proceedings of 15th International Symposium on the Packaging and Transportation of Radioactive Materials (PATRAM 2007). Miami, Florida, USA, Conference 2007. p.1171-76.

6. Hyland RW. Homogeneous nucleation kinetics of Al_3Sc in a dilute Al-Sc alloy. Metall Mater Trans A 1992; 23: 1947-55.

7. Fuller CB, Seidman DN. Temporal evolution of the nanostructure of Al(Sc,Zr) alloys: Part II-coarsening of $Al_3(Sc_{1-x}Zr_x)$ precipitates. Acta Mater 2005; 53: 5415-28.

8. Yelagin VI, Zakharov VV, Pavlenko SG, Rostova TD. Influence of Zirconium Additions on Aging of Aluminum-Scandium Alloys(Translation). Phys Met Metallogr 1985; 60: 88-92.

9. Riddle YW, Sanders TH. A study of coarsening, recrystallization, and morphology of microstructure in Al-Sc-(Zr)-(Mg) alloys. Metall Mater Trans A 2004; 35: 341-50.

10. Belov NA, Alabin AN, Eskin DG, Istomin-Kastrovskii VV. Optimization of hardening of Al-Zr-Sc cast alloys. J Mater Sci 2006; 41: 5890-9.

11. Fuller CB, Seidman DN, Dunand DC. Creep properties of coarse-grained Al(Sc) alloys at 300°C. Scripta Mater 1999; 40: 691-6.

12. Fuller CB, Seidman DN, Dunand DC. Mechanical properties of Al(Sc,Zr) alloys at ambient and elevated temperatures. Acta Mater 2003; 51: 4803-14.

13. Marquis EA, Seidman DN, Dunand DC. Precipitation strengthening at ambient and elevated temperatures of heat-treatable Al(Sc) alloys. Acta Mater 2002; 50: 4021-35.

14. Lai J, Zhang Z, Chen XG. Precipitation strengthening of Al–B_4C metal matrix composites alloyed with Sc and Zr. J Alloys Compd 2013; 552: 227-35.

15. Qin J, Zhang Z, Chen XG. Mechanical Properties and Strengthening Mechanisms of Al-15 Pct B_4C Composites with Sc and Zr at Elevated Temperatures. Metall Mater Trans A. 2016; 47: 4694-708.

16. Lai J, Zhang Z, Chen XG. The thermal stability of mechanical properties of Al-B_4C composites alloyed with Sc and Zr at elevated temperatures. Mater Sci Eng A 2012; 532: 462-70.

17. Toropova LSED, Kharakterova ML, Dobatkina, TV. Advanced aluminum alloys containing scandium: structure and properties. Moscow, Russia: Gordon and Breach Science Publishers; 1998.

18. Qin J, Zhang Z, Chen XG. Effect of Hot Deformation on Microstructure and Mechanical Properties of Al-B_4C Composite Containing Sc. Mater Sci Forum 2014; 794-796: 821-826.

19. Lloyd D. Aspects of fracture in particulate reinforced metal matrix composites. Acta Mater 1991; 39 :59-71.

20. Llorca J, Martin A, Ruiz J, Elices M. Particulate fracture during deformation. Metall Trans A 1993; 24: 1575-88.

21. Mummery P, Derby B, Scruby C. Acoustic emission from particulate-reinforced metal matrix composites. Acta Mater 1993; 41: 1431-45.

22. Nutt S, Duva J. A failure mechanism in AlSiC composites. Scripta Mater 1986; 20: 1055-8.

23. Kamat S, Hirth J, Mehrabian R. Mechanical properties of particulate-reinforced aluminum-matrix composites. Acta Mater 1989; 37: 2395-402.

24. Whitehouse A, Clyne T. Cavity formation during tensile straining of particulate and short fibre metal matrix composites. Acta Mater 1993; 41: 1701-11.

25. Lai J, Zhang Z, Chen XG. Effect of Sc, Zr, and Ti on the interfacial reactions of the B_4C/Al system. J Mate Sci 2011; 46: 451-9.

26. Kaufman JG. Properties of aluminum alloys: tensile, creep, and fatigue data at high and low temperatures. USA: ASM International 1999.

27. Chen XG, St-Georges L, Roux M. Mechanical Behavior of High Boron Content Al-B_4C Metal Matrix Composites at Elevated Temperatures. Mater Sci Forum 2012; 706-709: 631-7.

28. Tahamtan S, Emamy M, Halvaee A. Effects of reinforcing particle size and interface bonding strength on tensile properties and fracture behavior of Al-A206/alumina micro/nanocomposites. J Compos Mater 2014; 48: 3331-46.

29. Davidson DL. Tensile deformation and fracture toughness of 2014+15vol Pct SiC particulate composite. Metall Mater Trans A 1991; 22: 113-23.

30. Bhanuprasad V, Staley M, Ramakrishnan P, Mahajan Y. Fractography of metal matrix composites. Key Eng Mater 1995; 104: 495-506.